Biochimica et Biophysica Acta 1861 (2017) 3651–3660

Contents lists available at ScienceDirect

Biochimica et Biophysica Acta

journal homepage: www.elsevier.com/locate/bbagen

Inelastic and quasi-elastic neutron scattering spectrometers in J-PARC☆

H. Seto [a,*], S. Itoh [a], T. Yokoo [a], H. Endo [a], K. Nakajima [b], K. Shibata [b], R. Kajimoto [b], S. Ohira-Kawamura [b], M. Nakamura [b], Y. Kawakita [b], H. Nakagawa [c], T. Yamada [d]

[a] J-PARC Center, High Energy Accelerator Research Organization, 203-1 Shirakata, Tokai 319-1106, Japan
[b] J-PARC Center, Japan Atomic Energy Agency, 2-4 Shirakata, Tokai 319-1195, Japan
[c] MSRC, Japan Atomic Energy Agency, 2-4 Shirakata, Tokai 319-1195, Japan
[d] CROSS Tokai, 162-1 Shirakata, Tokai 319-1106, Japan

ARTICLE INFO

Article history:
Received 25 January 2016
Received in revised form 21 April 2016
Accepted 22 April 2016
Available online 6 May 2016

Keywords:
Inelastic neutron scattering
Quasi-elastic neutron scattering
Dynamical behavior
Chopper spectrometer
Backscattering spectrometer
Neutron spin echo spectrometer
2010 MSC: 00-01, 99-00

ABSTRACT

J-PARC, Japan Proton Accelerator Research Complex provides short pulse proton beam at a repetition rate 25 Hz and the maximum power is expected to be 1 MW. Materials and Life Science Experimental Facility (MLF) has 23 neutron beam ports and 21 instruments have already been operated or under construction/commissioning. There are 6 inelastic/quasi-elastic neutron scattering spectrometers and the complementary use of these spectrometers will open new insight for life science.
This article is part of a Special Issue entitled "Science for Life" Guest Editor: Dr. Austen Angell, Dr. Salvatore Magazù and Dr. Federica Migliardo.

1. Introduction

J-PARC, Japan Proton Accelerator Research Complex, aims to pursue frontier science in particle physics, nuclear physics, materials science, life science and nuclear technology. The accelerator complex consists of accelerators as follows; 400 MeV Linac, 3 GeV rapid cycle synchrotron ring (RCS) providing proton beams at 333 μA, and 50 GeV main ring (MR) providing proton beams at 15 μA. The beam from the RCS is injected to the Materials and Life Science Experimental Facility (MLF). The beam power has achieved at 500 kW in 2015 and will be increased up to 1 MW within some years. The construction of 21 neutron instruments has been completed; 19 instruments are opened for users, 2 are under commissioning as shown in Fig. 1.

There are 6 inelastic neutron scattering (INS) and quasi-elastic neutron scattering (QENS) instruments in MLF. 4SEASONS and HRC are Fermi chopper type direct geometry spectrometers, and AMATERAS is one of a disk chopper type. POLANO is a chopper spectrometer capable to use polarized neutron. DNA is a near-back scattering spectrometer with a pulse-shaping chopper, and available to measure at μeV resolution. Neutron spin echo spectrometer VIN ROSE includes 2 instruments, MIEZE (Modulated Intensity with Zero Effort) type and NRSE (Neutron Resonance Spin Echo) type. Among them, 4SEASONS, AMATERAS, HRC, and DNA are opened for users, VIN ROSE is now under commissioning and POLANO is almost ready for accepting the first beam. By the combination of these instruments, a very wide Energy-Momentum Transfer space is covered as shown in Fig. 2. With these instruments, MLF gives opportunities to perform experiments in widely spread fields including solid state physics, amorphous materials and liquids, soft and biological matters, as well as industrial applications such as tire rubbers and battery materials.

In this article, we review the characteristic features and the present status of these 6 instruments for INS and QENS. Additionally, 2 bio-related experimental results obtained from MLF spectrometers are shown.

2. Neutron source characteristics

Designed maximum power of J-PARC is 1 MW at the repetition rate of 25 Hz. The proton beam is injected to mercury target at 333 μA and 3 GeV from RCS with an effective time width of 1 μs two bunches with 150 ns width separated by 750 ns [1].

One of the most important results of cooperation between the accelerator team and the neutron team is an introduction of a master clock for the accelerator control. Now the accelerator control is extremely accurate with a master clock of 12 MHz with time jitter of 1.7 ns [2]. This scheme is quite important for instrument control, especially chopper control. We require a time jitter less than 0.3 μs for a

☆ "This article is part of a Special Issue entitled "Science for Life" Guest Editor: Dr. Austen Angell, Dr. Salvatore Magazù and Dr. Federica Migliardo".

* Corresponding author.

http://dx.doi.org/10.1016/j.bbagen.2016.04.025

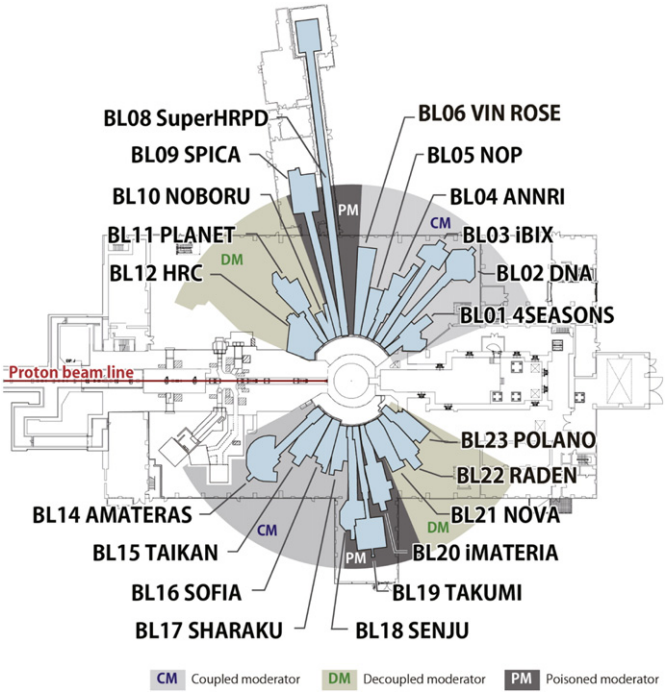

Fig. 1. Neutron instruments in Materials and Life Science Experimental Facility, J-PARC.

Fermi chopper phase-control above 1 eV neutrons, where the intrinsic time width from moderator follows $\Delta t_m[\mu s] = 2/\sqrt{E_i[\mathrm{eV}]}$ [3].

The repetition rate of 25 Hz gives a wide dynamic range in one frame for time-of-flight (TOF) instruments and high pulse-peak intensity. This choice again gave a burden for accelerator and target technology; one proton bunch contains larger number of protons than that for higher frequency, giving a higher space-charge effect and a worse damage in the neutron target.

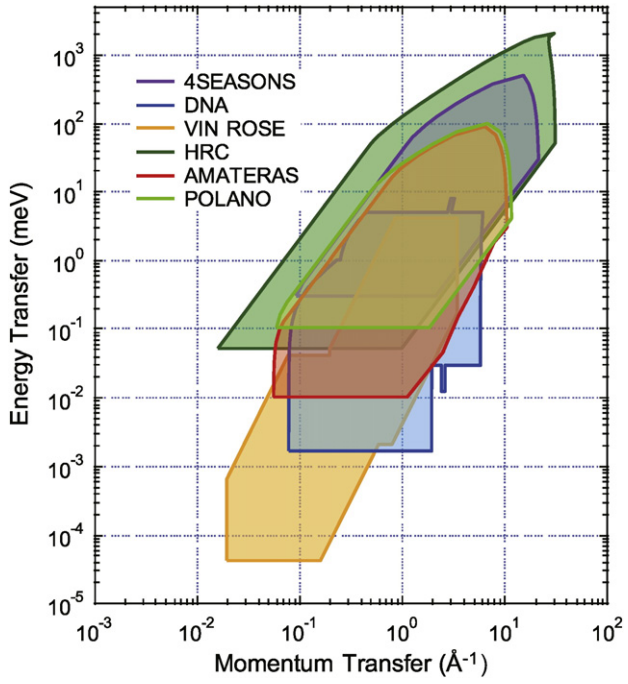

Fig. 2. Energy-Momentum Transfer space covered by the inelastic and quasi elastic neutron scattering instruments in MLF.

For a typical instrument with 20 m flight path, the dynamical range is about 8 Å in the wave length, or from 1 meV to 10 eV in energy. This repetition rate is a great compromise to satisfy the requirements of both high energy spectroscopy and slow neutron experiments, and it is also good for high resolution instruments with a long flight path.

When protons injected to the target, high energy neutrons are created and scattered to whole solid angle. Some of neutrons are scattered backward by reflector and go into a moderator, where neutrons loose energy by scattering from hydrogenous materials, and are cooled down to the moderator temperature suitable for scattering experiments.

MLF has three cryogenic super-critical hydrogen moderators (20 K, 1.5 MPa) [4]. The coupled moderator (CM) which gives high intensity with a broad peak structure, is surrounded by an ambient water premoderator to slow down high energy neutrons and remove unnecessary heat deposit before neutrons go into CM. Since CM occupies the optimized space below the target by itself, its performance is quite outstanding. A decoupled moderator (DM) and a poisoned decoupled moderator (PM) produce sharp pulse structure and are suited to medium resolution and high resolution instruments, respectively. Details of the pulse shape from the moderators are described in Ref. [5].

Fig. 3 shows calculated peak structure for each moderator at $E_i =$ 5 meV. Broadness and high intensity of CM are much enhanced at low energy below around 30 meV. At higher energy the peak structure becomes similar to each other among the moderators. The sharp pulse from the neutron source and the utilization of pulse shapers provides practically symmetric resolution function for each spectrometer installed at MLF.

3. Chopper spectrometers

3.1. 4SEASONS

4SEASONS is a thermal neutron Fermi chopper spectrometer designed for measurements of dynamics in the 10^0–10^2 meV energy range [6], which is one of the Public Beamlines in MLF. A schematic view of 4SEASONS is presented in Fig. 4. It is installed at BL01 beam port viewing CM. Neutrons are transported to a sample position, which is located at 18 m downstream from the moderator, through an elliptically converging straight neutron guide tube coated with supermirrors. The incident neutrons are monochromatized by a fast-rotating Fermi chopper positioned at 1.7 m upstream from the sample

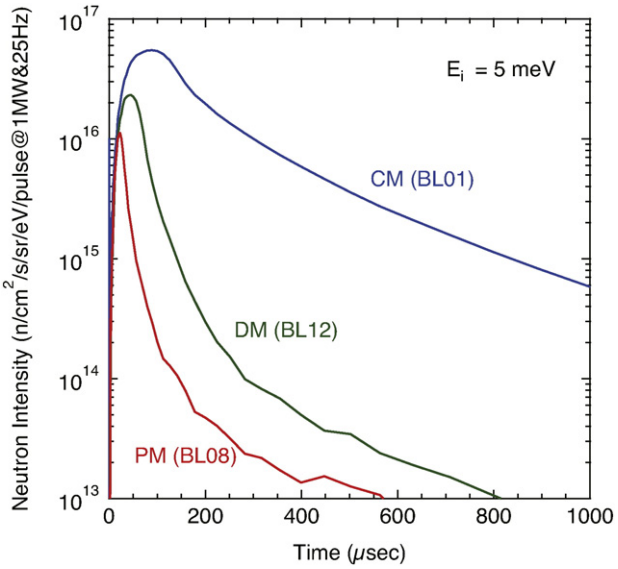

Fig. 3. Typical pulse structures of neutrons from CM, DM, and PM.

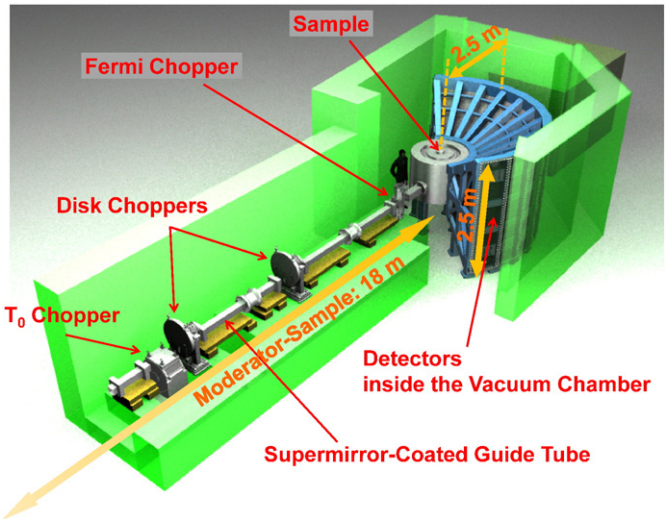

Fig. 4. Schematic view of 4SEASONS.

position. In addition, the instrument has a T0 chopper for suppressing fast neutrons and two disk choppers for band definition. Scattered neutrons are detected over time by the ^{3}He position sensitive detectors placed at 2.5 m from the sample position. The angular coverage of the detectors relative to the direct beam is from −35° to +91° horizontally and from −25° to +27° vertically. The event-recorded data are converted to the dynamical structure factor by the software package Utsusemi [7].

4SEASONS was originally developed to investigate high critical-temperature (high-T_c) oxide superconductors. To observe weak inelastic signals from these materials, the instrument is designed to supply high thermal neutron flux by relaxing the resolution. The available neutron flux and resolution depend on the rotation speed of the Fermi chopper. Expected neutron flux at the sample position at 1 MW, energy and momentum transfer resolutions at the elastic scattering condition are ~10^5 neutrons/(cm^2 s), 6% relative to the incident energy and 1–2% relative to the incident wave number, respectively [6,8]. The instrument is optimized for the sample size of 20 mm × 20 mm, though the actual beam size is about 35 mm × 35 mm. Another important feature of 4SEASONS is that it can simultaneously perform measurements at multiple incident energies (Multi-E_i measurements) [9] by taking advantage of the fact that the chopper rotates considerably faster than the repetition rate of the neutron source [10,11]. The practical number of available incident energies is 3–4, which covers one or two orders of magnitude energy scale depending on an experimental condition [12]. Thanks to its high flux and high measurement efficiency, 4SEASONS can perform measurements which had been too time-consuming and considered unrealistic on conventional INS instruments.

One of the typical kind of measurements is four-dimensional mapping of the Energy-Momentum Transfer space in a single crystal by rotating the crystal. Fig. 5 shows an example of the rotating-crystal measurement. It shows two-dimensional maps of four-dimensional phonon spectrum in copper as cuts on the (*H*,*K*,*K*), *H*-ω, and *K*-ω planes. This four-dimensional spectrum can be obtained within a reasonable measurement time (a few days). This kind of measurement occupies a large portion of the recent experiments performed on 4SEASONS.

The major research fields on 4SEASONS are strongly correlated electron systems and magnetism. Indeed, these research fields dominated 70% of the General Use proposals in 2014. This trend seems natural considering the original research target of the instrument. However, it should be noted that a sizable number of proposals belong to the other research fields such as thermoelectric materials, catalysts, and hydrides. We also note that the high-energy INS experiments provided by 4SEASONS should be effective to investigate dynamical behaviors of light elements because the vibrational frequency is inversely proportional to the square root of the reduced mass. In fact, the O–H stretching vibration in water exhibits an energy band around 400 meV. Thus, we stress that 4SEASONS has a potential to contribute biology by investigating dynamical behavior of hydrogen.

3.2. AMATERAS

AMATERAS (Fig. 6) is a cold-neutron multi disk chopper spectrometer installed at BL14 viewing CM [14,15]. The spectrometer is designed to cover the energy range from cold to sub-thermal region and is dedicated to INS and QENS experiments on single-crystals, powder, liquid and amorphous materials to study the various subjects, i.e., collective excitations from structural and magnetic fluctuations in solid, diffusion of ions or molecules in liquids, and dynamics in polymers and biological materials. It was designed to utilize incident neutron energy from 1 to 80 meV. The fine energy resolution can be obtained in the lower energy region. For example, the achievable finest energy resolution is $\Delta E/E_i \leq 1\%$ at $E_i = 20$ meV, and it could be less than 0.6% at $E_i = 1$ meV. The maximum neutron flux at the sample position is obtained at $E_i = 11.5$ meV. Therefore, we can say that the best performance of this spectrometer is realized at this energy range, while still reasonable energy resolution and intensity is available up to 80 meV. The designed momentum transfer resolution ($\Delta Q/k_i$) is between 2% and 0.2%. The estimated neutron flux at 1 MW is 3×10^4 neutrons/(cm^2 s) at $E_i = 20$ meV and $\Delta E/E_i = 1\%$. However, the present neutron flux is much less than expected due to several reasons and we are making continuing effort to fix this problem [16]. The maximum sample size is 30 mmW × 50 mmH and the beam transport design is optimized for the sample size of 10 mmW × 20 mmH. AMATERAS has a relatively long flight path of 30 m from the source to a sample position. This flight path is equipped with a supermirror beam transport, which has curved section in horizontal and is combination of parabola and straight sections in vertical. The sample position is surrounded by 448 (at the full installation) 3 m long and 1 in. diameter ^{3}He 1D position sensitive detectors, which are placed at 4 m away from the sample position (at the equatorial position). The angular coverage of the detectors is from −40° to 140° horizontally and from −16° to 22° vertically at the full installation, however, currently the detector bank is partly filled from 5° to 112° horizontally and from −16° to 22° vertically. On the beam line, 3 sets of fast disk choppers and 2 sets of slow disk choppers are placed.

One of the most characteristic feature of AMATERAS is to utilize the pulse-shaping technique, which is also employed by LET at ISIS [17] and CNCS at SNS [18]. One set of fast disk choppers is located at the upstream position (7.1 m from the source) as a pulse shaper. The pulse shaper cuts out the ideal (sharp and symmetric) peak from the source pulse, which has a large intensity but broad and asymmetric pulse shape as mentioned above. By using a pulse shaper and owing to the high peak intensity from CM, AMATERAS is capable to perform fine and flexible energy resolution INS and QENS experiments with high intensity [15]. AMATERAS is designed to carry out the Multi-E_i measurements by using a repetition rate multiplication technique that was demonstrated on 4SEASONS for the first time [9], which is described in Chap. 3.1 in detail. This opportunity in INS and QENS experiments has triggered attempts to perform novel data analysis such as the mode-distribution analysis, which is a new approach to analyze QENS data without any assumptions of models [19].

The first phase of construction of the spectrometer was finished in the spring of 2009 with 60% filling of the detector banks, and was opened for general users from December 2009. Until the end of 2015, AMATERAS carried out more than 80 proposals in various research fields. The majority of research subjects is solid state physics especially magnetism in most of cases. Amorphous, liquid, soft and biological materials are also often measured as exemplified in Chap. 6.1. Not a small number of experiments on industrial applications, studying dynamics

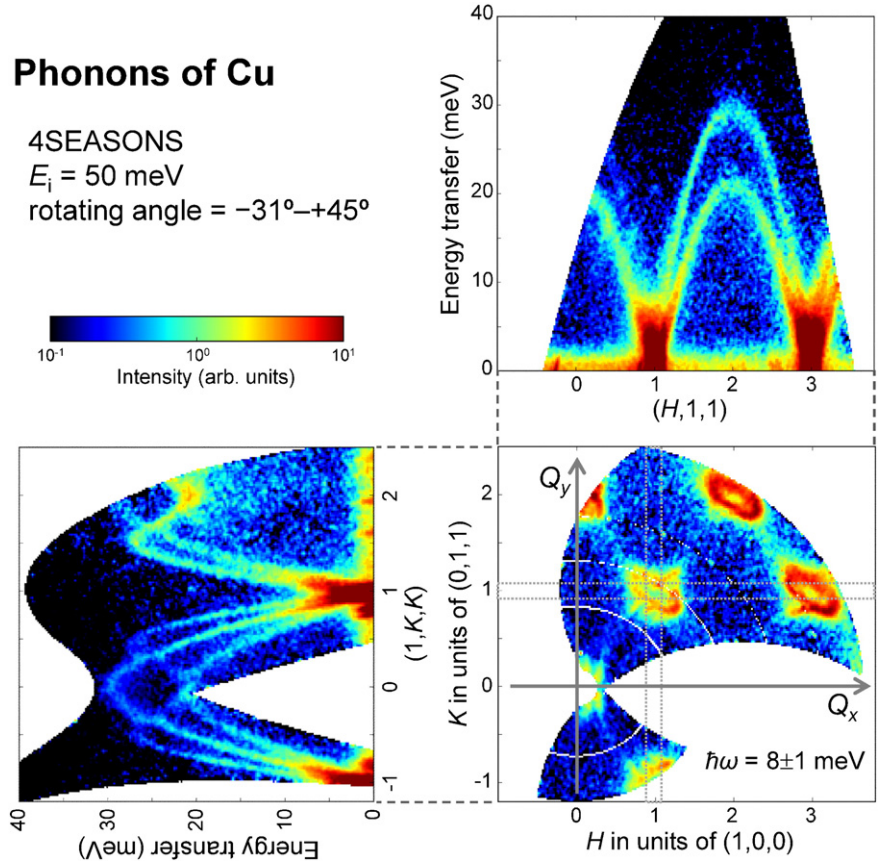

Fig. 5. Four-dimensional mapping of the phonon spectrum in a copper single crystal obtained by a measurement with rotating crystal over 76° [13]. Utilized incident energy is 50 meV. The sample volume is 4.2 cm^3. The total measurement time is 17.5 h at the proton beam power of 300 kW. The crystal was provided by Prof. Y. Yamaguchi at Tohoku University.

for development of polymer products, battery materials and etc., have also been carried out.

3.3. HRC

The High Resolution Chopper Spectrometer (HRC) at BL12 viewing DM delivers high-resolutions and relatively high-energy neutrons for a wide range of studies on the dynamics of materials [20]. As shown in Fig. 2, an energy range of E_i = 2–2000 meV is available, and especially by using E_i < 300 meV, energy resolution of $\Delta E/E_i$ = 2% can be achieved as the best resolution. A schematic layout of HRC is illustrated in Fig. 7. The primary flight path is 15 m, where a supermirror guide tube of 9.9 m long, a T0 chopper running up to 100 Hz at 9 m from the neutron source, a Fermi chopper at 14 m from the source, and an incident beam collimator system just at the upper stream of the sample are installed. HRC has a detector array of ^{3}He position sensitive detectors of 2.8 m long and 3/4 in. diameter located at 4 m from the sample position covering scattering angles up to 62° for conventional experiments, also another detector array of ^{3}He position sensitive detectors of 0.8 m

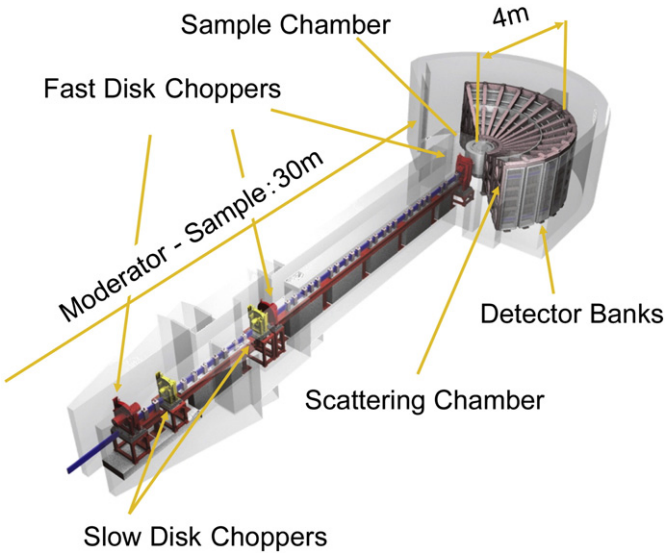

Fig. 6. Schematic view of AMATERAS.

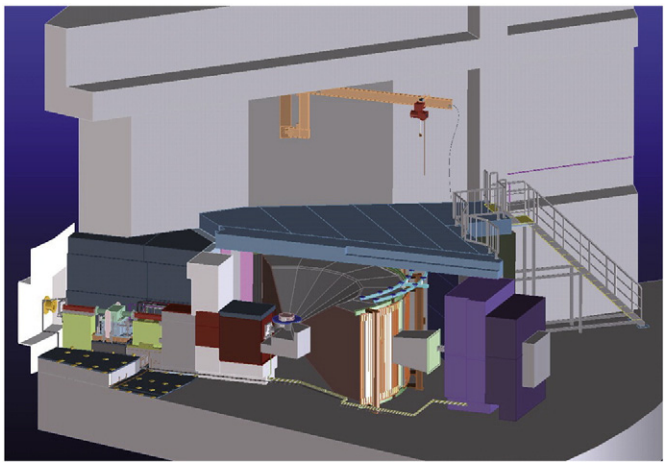

Fig. 7. Schematic view of HRC.

long and 1/2 in. diameter at 5.2 m down to 0.6°. An available sample size is up to 50 mm × 50 mm for conventional experiments, and 30 mm × 30 mm for low angle experiments. A designed neutron flux at the sample position is 2×10^5 neutrons/(cm^2 s) for $E_i = 100$ meV with $\Delta E/E_i = 2.5\%$ at 1 MW [20]. The neutron flux for low angle experiments is reduced to 1/4 of that for conventional experiments by using the incident beam collimator with a fine collimation. The incident beam collimator system having two collimators composed of slits of vertical sheets of Cd is installed for background reduction and one from the two is selected: a coarse collimation of 1.5° for conventional experiments using detectors down to 3° and a fine collimation of 0.3° for low angle experiments using detectors down to 0.6°. On HRC, three types of INS experiments can be performed: high-resolution experiments in a conventional Energy-Momentum Transfer space, Neutron Brillouin Scattering (NBS), and eV neutron spectroscopy [20]. The dynamical structure factor in a spin system can be determined in the full Energy-Momentum Transfer space with conventional experiments, and ferromagnetic spin waves and acoustic phonons can be observed by using a polycrystalline or liquid sample with NBS.

Among them, NBS on HRC is described. Owing to the kinematic constraints of neutron spectroscopy, incident neutron energy in the sub-eV region with a high resolution is necessary, and the scattered neutrons need to be detected at very low scattering angles down to 0.6°, for measuring the scattering near to the forward direction. On HRC, NBS experiments became feasible by reducing the background noise at low scattering angles [21,22]. The NBS option makes HRC different from 4SEASONS and AMATERAS. The principle of NBS is not new [23,24,25], and the Energy-Momentum Transfer space accessible by NBS has been extended by utilizing higher energy neutrons in spectrometers such as BRISP spectrometer at ILL [26]. An example of NBS on HRC is shown here. We observed spin waves in a polycrystalline sample of a well-known cubic perovskite ferromagnet, $La_{0.8}Sr_{0.2}MnO_3$, of which Curie temperature is 316 K [27]. Fig. 8(a) shows a raw spectrum from the sample, a background spectrum form the empty can, and the background-subtracted spectrum at a selected Q. The background-subtracted spectrum can be well fitted with the sum of resolution-limited spin wave peaks including the temperature factor and an elastic Gaussian peak [21]. Note that the magnetic scattering is dominant in this Q range, because the magnetic form factor shows the maximum intensity and the phonon intensity reduces as the Q^2 dependence. The obtained peak positions of the spin waves are plotted in Fig. 8(b). The dispersion relation at 245 K was well fitted to $E(Q) = DQ^2$ with the energy transfer E and the scattering vector Q (Fig. 8(b)). The D value was obtained to be 88 ± 2 meVÅ^2, which agreed well with the previous INS result using a single crystal [27]. This result confirms again that the magnetic scattering is dominant in this Q range. In this way, the NBS method became successfully feasible on HRC [21,22]. Next, spin waves in another polycrystalline sample of a cubic perovskite, $SrRuO_3$, which is a metallic ferromagnet showing anomalous Hall effect [28], were measured in exactly the same manner as that for $La_{0.8}Sr_{0.2}MnO_3$. A large single crystal of this material suitable for INS experiments has not yet been synthesized. As shown in Fig. 8(b), the observed spin wave dispersion relation at 7 K was well fitted to $E(Q) = E_g + DQ^2$ with an apparent energy gap E_g [21]. We clearly found the energy gap by accessing the low Q by the NBS method.

The NBS method gives opportunities to investigate dynamical behavior of biological molecules and solvent. Recent experiments on hydrated β–lactoglobulin powder show well-defined dispersive excitation at low-Q [29]. The experimental results will appear elsewhere after finishing the data analysis.

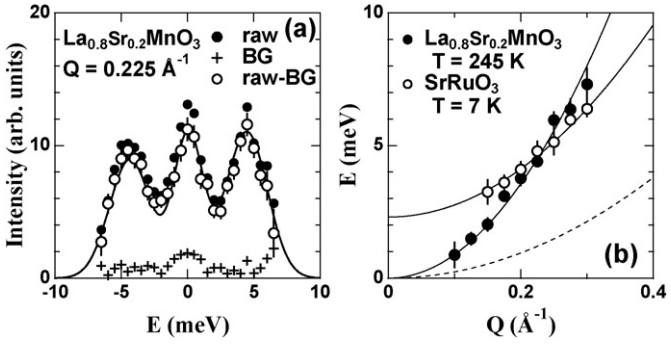

Fig. 8. INS spectrum from $La_{0.8}Sr_{0.2}MnO_3$ at $Q = 0.225$ Å^{-1} at $T = 245$ K: raw spectrum, background and the subtraction (a). The solid line is the fitted curve to the subtraction with resolution-limited spin waves adding an elastic Gaussian peak. Dispersion relations of spin waves in $La_{0.8}Sr_{0.2}MnO_3$ and $SrRuO_3$ (b). The solid lines are fitted curves. The dashed line is the upper limit of scan area for a spectrometer with the lowest scattering angle of 5°.

3.4. POLANO

POLANO (polarized neutron spectrometer) is one of the youngest generation instruments in MLF, and constructed at BL23 viewing DM [30,31,32].

In MLF, three direct geometry spectrometers are now part of the research program as mentioned above to survey the lattice vibration, spin dynamics, electronic orbital motions and so forth. POLANO was designed as one of the "chopper type" spectrometer while the other three instruments have no polarization analysis capability. Although the polarized neutron technique has been developed and used for many years, the application of the TOF method has only been realized in recent years. In particular, with regard to the inelastic spectrometer, the polarized neutron technique finds limited practical use in wide scattering angle instruments. In the light of recent discoveries in material science, many of the observed complex phenomena are largely due to the entangled physical degrees of freedom (spins, charges, orbitals, and even lattice vibration). A unique, effective, and direct way to observe these polarizations separately is via the polarization analysis.

POLANO is a collaborative project between KEK and Tohoku University. Our principal concept is to achieve higher energy polarization analysis of inelastic scattering beyond the reactor based neutron source. The schematic view of the instrument is depicted in Fig. 9.

Since the designing concepts of POLANO are compact with reasonably wide sample space design, higher neutron flux, higher neutron energy polarization up to 100 ~ 120 meV, and medium resolution, the parameters L1 (moderator − sample distance) = 17.5 m, L2 (sample − detector distance) = 2.5 m and L3 (Fermi chopper − sample distance) = 1.85 m were chosen. Viewing DM with these geometrical conditions yields 4% of energy resolution ($\Delta E/E_i$) and 1 ~ 2% of momentum resolution ($\Delta Q/k_i$) at elastic position. Expected momentum transfer is up to the range of 12 Å^{-1} with 100 meV incident energy, covering almost all the interesting E–Q space as shown in Fig. 2. The optimum beam size is 20 mm × 20 mm at the sample position.

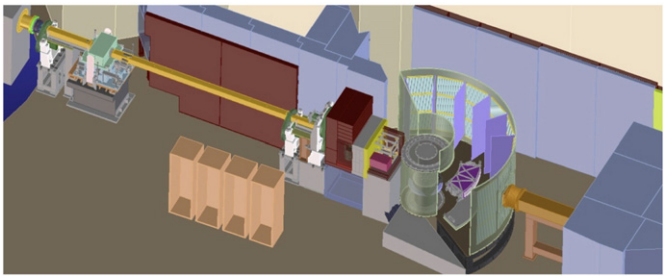

Fig. 9. Schematic view of POLANO spectrometer.

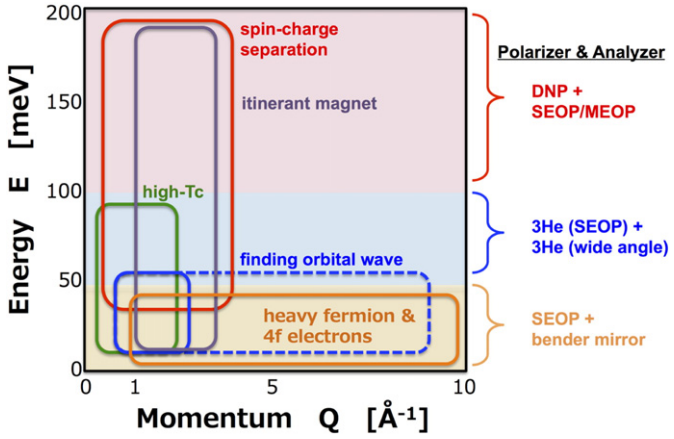

Fig. 10. Expected Q and E diagram.

We start the spin polarization experiment up to $E_f < 50$ meV as the first step. Fig. 10 shows the momentum and energy diagram for the expected Q–E range in POLANO. Since the energy scale in heavy fermion or 4*f* electron systems is relatively low, it is one of themes carried out in the beginning. The searching of the direct evidence for orbital waves and multiferroic material will be the target to be explored. With developing wide angle spin exchange optical pumping (SEOP) device, energy range will be expanded up to approximately 120 meV entering upon a new paradigm for neutron polarization analysis. The reactor based instruments no longer reach this high energy, and scheduled accelerator based instruments are designed for lower energy range (cold neutrons). Many of phonon frequencies (Debye frequencies) are within this energy range in solid state materials. Even the high-T_c superconductivity will be objective. Hydrogen science can also be the target of research with neutron polarization analysis since the local vibrational motion of hydrogen in most metal hydrides is roughly estimated in the energy range of 70–150 meV. The combination of the spin contrast variation technique and the inelastic neutron scattering may give opportunities to investigate hydrogen dynamics selectively from complex systems such as protein and tire rubber [33,34].

We expect to realize neutron polarization at much higher energy as a final step. This needs revolutionary techniques in order to polarize sub eV neutron spins, such as dynamical neutron polarization (DNP) or high polarization SEOP/MEOP. Once we obtain these high-energy neutron polarization technique, research on itinerant electron system and spin-charge separation in strongly correlated electron system like cuprates will make remarkable progress.

4. Backscattering spectrometer

4.1. DNA

A TOF near-backscattering spectrometer (n-BSS), DNA, was constructed at BL02 and started operation in early 2012. It is an indirect geometry instrument with Si crystal analyzers receiving the neutron beam from CM. Aiming for a high energy resolution even with high intensity, DNA is the first n-BSS equipped with a high-speed pulse-shaping disk chopper at a spallation pulsed neutron source over the world [35]. The construction purpose of DNA is to explore, in nanosecond timescale or in μeV energy region, dynamical behaviors of atoms and spins in bio-molecules [36], soft matters, strongly-correlated electron systems and so on.

In the following part, a brief outline of DNA is indicated. The detailed specifications for DNA was reported elsewhere [35].

An overview of DNA is shown in Fig. 11(a). The pulse-shaping chopper is the first key device for DNA. The pulse width is selectable by changing the slit width and the rotational speed of the chopper disk. This allows us to adjust rather flexibly the energy resolution and the measurable intensity according to sample quantity and aiming science. Si crystal analyzer is the second key device for DNA. The Si(111) crystal analyzers were installed in the vacuum vessel covering the scattering-angle ranges from −30° to +150° horizontally and from +21° to −14° vertically (Fig. 12). The spherical analyzer surface is divided to the upper and the lower parts. Scattered neutrons are measured by position-sensitive ^{3}He gas detectors (PSD) arranged on the same circumference of the scattering center upward and downward shifted, after being energy-analyzed (near back-scattered at Bragg angle $\theta_B \sim 87.5°$) by the upper and the lower parts of the crystal analyzer units, respectively (Fig. 11(b)). These arrangements of the analyzer units and the detectors enable us to angle-resolve scattered neutrons in horizontal and vertical directions two-dimensionally, and therefore, this spectrometer has a potential to conduct experiment even for a single crystalline sample.

Because of the optimal combination of the major spectroscopic devices: pulse shaping chopper, Si crystal analyzer and so on, it became possible to measure dynamical structure factor $S(Q,E)$ with μeV energy resolution (the best resolution is about 2.4 μeV by operating a pulse shaping double disk chopper at 225 Hz whose phase is optimized to the narrowest slit of 10 mm width) and high neutron flux (estimated maximum flux at 1 MW is 1.5×10^8 neutrons/(cm^2 s)) at the sample position and quite low instrumental background, i. e., the signal to noise ratio (S/N) is about 10^5. Note that the general S/N values of back scattering spectrometers installed in other facilities are between 3000 and 1700. Taking advantage of this feature, the research fields is widely expanded not only for QENS but also for INS with very precise energy

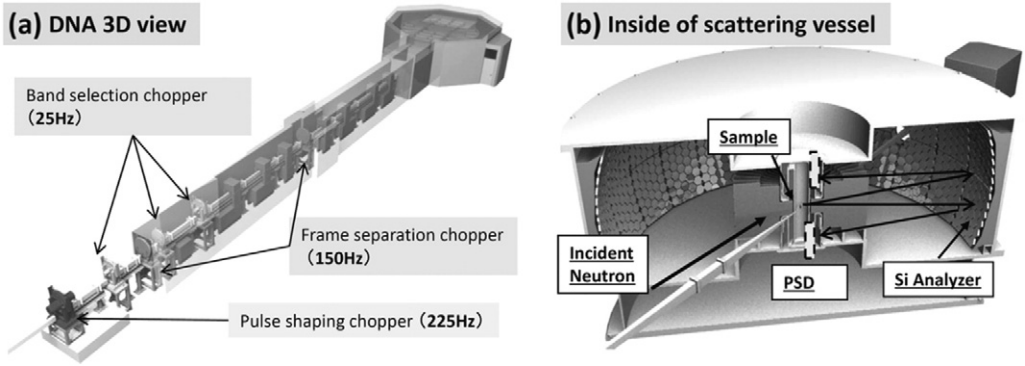

Fig. 11. (a) Schematic view of DNA spectrometer. Six disk choppers of three types are installed on the neutron super mirror guide beamline. By the pulse shaping chopper installed in the closest position to the neutron source, a wide neutron pulse generated from CM, becomes the sharp pulse. (b) Inside of DNA scattering vessel. At the end of neutron guide, the incident neutron beam was focused on the sample position. The energy of scattered neutron at sample was selected by Bragg reflection of Si analyzer, after that the scattered neutron was detected by position sensitive ^{3}He gas detectors (PSD).

Fig. 12. Si(111) analyzer banks (from left side to center) and the position sensitive 3He gas detector (PSD)-amplifier units (right side) in DNA vacuum vessel. Sample position is at the center of PSD-amplifier units.

resolution. This spectrometer is suitable to investigate dynamical behaviors of proteins, for example, human α-synuclein which form amyloid fibrils [36,37]. The elucidation of low-energy dynamics of proteins at low temperature is also expected. Additionally, experimental proposals from research field of strongly-correlated electron systems are increasing to investigate low-energy excitations around 1 μeV at low temperatures around 10 mK. Therefore, it is urgent issue to introduce cryogenic equipment such as a dilution refrigerator as a sample environment.

5. Neutron spin echo spectrometer

5.1. VIN ROSE

The neutron spin echo (NSE) technique is an essential spectroscopic method, which at present time has achieved the highest energy resolution [38]. NSE with a pulsed neutron source makes it possible to scan very efficiently a wide spatiotemporal space. Kyoto University and KEK have been installing jointly two types of NSE spectrometers at BL06 viewing CM since 2011, that is, a neutron resonance spin echo (NRSE) instrument and a modulated intensity by zero effort (MIEZE) instrument. One of the characteristics of the instruments is the use of resonance spin flippers that make it possible to install compact and multiple spectrometers in a limited space. Another characteristic feature is an adoption of two curved guides in order to expand experimental space for two spectrometers and transport optimized neutron beam. By using the curved guide tubes, fast neutrons and gamma rays from the source are stopped by an iron beam dump at the upstream part of the instruments. The beam line has been named "VIN ROSE" (VIllage of Neutron ResOnance Spin Echo Spectrometers), which will spawn a new field of spectroscopic methods [39]. Fig. 13 shows the schematic view of VIN ROSE.

NRSE is suitable to study slow dynamics of soft matter with high energy resolution. The most successful application of neutron spin echo spectroscopy is those on polymer systems which was reviewed in ref. [40], and further references are therein. While, MIEZE has a big advantage of flexible sample environments with potential to open new fields of study such as spin dynamics in strongly correlated systems [41,42,43]. The designed dynamic range of MIEZE is $0.2 < Q < 3.5$ Å^{-1} and $0.001 < t < 2$ ns, and that of NRSE is $0.02 < Q < 0.65$Å^{-1} and $0.1 < t < 100$ ns, respectivly.

The key components of the spectrometers are neutron optical devices. All the supermirrors for the guides are deposited on silicon wafers with thickness of 3 mm by using the ion beam sputtering machine at Kyoto University Research Reactor Institute [44,45]. The neutron guide for NRSE and that for MIEZE use $Q_c = 2.5$ and 3 supermirrors, respectively. The supermirrors were held precisely and covered by iron shields to reduce dose level. Their high performance has been proven by neutron reflectivity measurements etc.

VIN ROSE has accepted neutron beams since April 2014. After that, the performance of the installed neutron guides was tested with several methods. In the case of NRSE, observed value at the guide-end positoin agreed well (95%) with a calculated value (6.9×10^8 neutrons/(cm^2 s) at 1 MW), on the other hand, the agreement was 56% for MIEZE (2.7×10^8 neutrons/(cm^2 s) at 1 MW). At this moment, we are carefully considering the reasons, which may originate from misalignment of the mirrors, deflection of the mirrors, etc. [45].

After the investigation of the neutron guide performance, we installed the components (a polarizer, two resonance spin flippers, and an analyzer) in MIEZE to observe the neutron spin echo signals. The combination of MIEZE and TOF is a quite new method, and the related previous studies were just tentative [46,47]. Therefore, the quantitative verification of TOF-MIEZE is necessary and expected in the near future. We were able to measure successfully TOF-MIEZE signals with several different conditions, and the quantitative analyses of the TOF-MIEZE signals are currently proceeding [45]. The user program of VIN ROSE is planned to start from FY2017, between April 2017 and March 2018.

6. Scientific results

6.1. Deoxyribonucleic acid (DNA) rigidity

The genomes (DNA sequences) of many organisms have been obtained. While amino acid sequences of proteins are encoded in DNA (deoxyribonucleic acid), noncoding genomic DNA regions are known to regulate gene expression through DNA-protein interactions. Recent studies have shown that not only a direct interaction between protein and DNA (known as "direct recognition") but also an "indirect recognition", which is an easy transformation of the sequence-dependent DNA structure, are important to transcript the information contained in

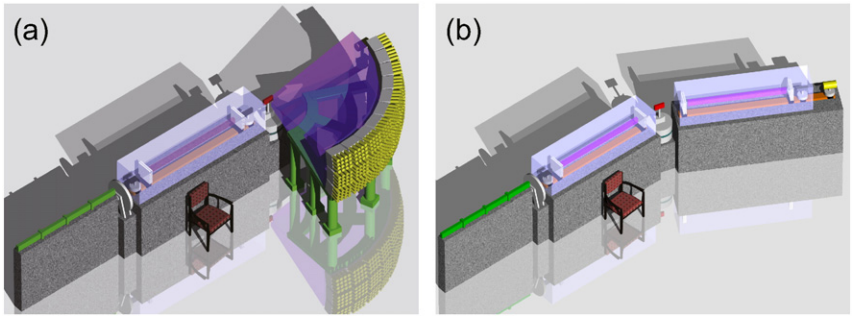

Fig. 13. Schematic view of VIN ROSE. (a) MIEZE type, (b) NRSE type.

genomes. Because the sequence-dependent DNA fluctuation in the process of indirect recognition is essential, it is necessary to demonstrate the dynamical behavior of DNA experimentally [48]. In the previous computational studies, it was predicted that a dodecameric DNA of 5′ CGCGAATTCGCG3′ (AATT) is more rigid than that of 5′CGCGTTAACG CG3′ (TTAA) [48]. QENS was expected to give a direct evidence for the difference of DNA rigidities depending on the base sequences, but the difference of QENS spectra were very small and the evaluation of the DNA rigidities were not succeeded so far. Here, we emphasize that the high-intensity neutron source and the chopper spectrometer in MLF enable us to pursue this research [49].

The dynamical behaviors of two DNA sequences (AATT and TTAA) were investigated using AMATERAS with the incident energy of 3.132 meV and the energy resolution of 28 μeV. H/D-exchanged DNA powder samples hydrated by equilibrating with KCl-saturated D_2O solution were used for both sequences, where DNA take B-form helix. The measurement time was between 5 and 8 h. Each sample was stuffed in a hollow aluminum container of 10.0 mm external radius and the height of the sample holder was 30 mm. QENS spectrum of AATT sequence is shown in Fig. 14(a). The difference between the neutron spectra from AATT and TTAA sequences actually was not so large. In the data analysis, at first, the raw data have been examined carefully in order to judge whether two spectra are different or not considering the effect of background. Fig. 14(b) shows the ratio $S(Q,\omega)_{TTAA}/S(Q,\omega)_{AATT}-1$ to compare the neutron spectra. There is significant deviation from zero in the inelastic region and the deviation is symmetric. This result suggests that the difference between these two spectra comes from the intensity and/or the width of QENS; the quasi-elastic scattering from TTAA is more significant than that from AATT. Then, in order to examine the difference quantitatively, the data were analyzed by the fitting with the sum of a delta function and a Lorentzian function.

Examining the half-width at half maximum (HWHM) of the QENS spectra as a function of Q gives information on relaxation time of DNA fluctuations. Fig. 15 shows the HWHM's of both the DNA dodecamers. HWHM increases with Q^2 at the lower Q region, and asymptotically approaches a constant value at large Q for both the sequences. In the low Q region, the HWHM's are almost the same, while, the constant value in the high Q region of TTAA was larger than that of AATT. This indicates that the diffusive motion is dominant with the similar frequency for both the sequences at longer length scales, whereas at shorter length scales, the frequency of motion of TTAA is larger than that of AATT. The plateau of HWHM at higher Q region indicates that the correlation times are independent of the length scale, suggesting that the jump motion

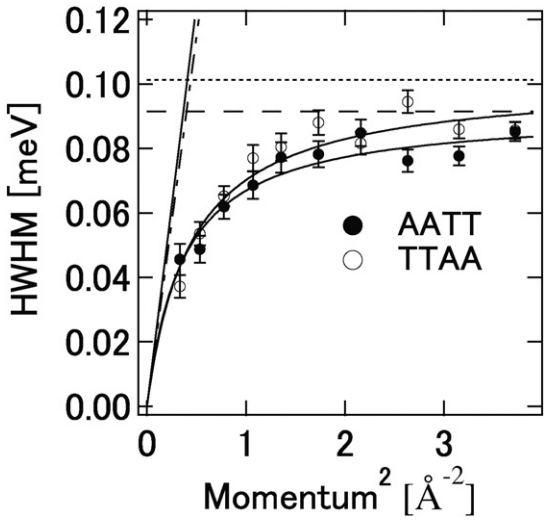

Fig. 15. HWHM's of QENS spectra of AATT and TTAA dodecamers. Lines from the origin indicate diffusion contributions (solid line: AATT, dot-dash line: TTAA). Horizontal lines indicate 1/Γ (dashed line: AATT, dotted line: TTAA).

dominates toward smaller length scales. Thus the behaviors are explained by the function of the jump diffusion model [50] as,

$$\Gamma(Q) = \hbar \frac{DQ^2}{1 + DQ^2\tau_0} \tag{1}$$

The diffusion coefficients, $6.0 \pm 0.8 \mathrm{nm^2 s^{-1}}$ for AATT and $5.5 \pm 0.5 \mathrm{nm^2 s^{-1}}$ for TTAA, are almost the same within the error. The residence time of a hydrogen atom is calculated as $\tau = 1/\Gamma(Q \to \infty)$, where $\Gamma(Q \to \infty)$ is HWHM obtained from the asymptotic behavior at higher Q. The resulting residence time for AATT, $\tau = 45.2 \pm 1.5$ ps, is longer than that of TTAA, $\tau = 40.9 \pm 1.1$ ps.

This result is consistent with the molecular dynamics simulation [48]. We certified experimentally that the indirect interaction depending on the DNA flexibility is important in the recognition of DNA, which has been proposed by the simulations and the statistical analyses of crystal structures [51]. This result demonstrates that genomes include informations of base sequences as well as the DNA flexibility. It is expected that the dynamical property of DNA will contribute to elucidate the mechanism of the "on/off switch" of the gene-expression.

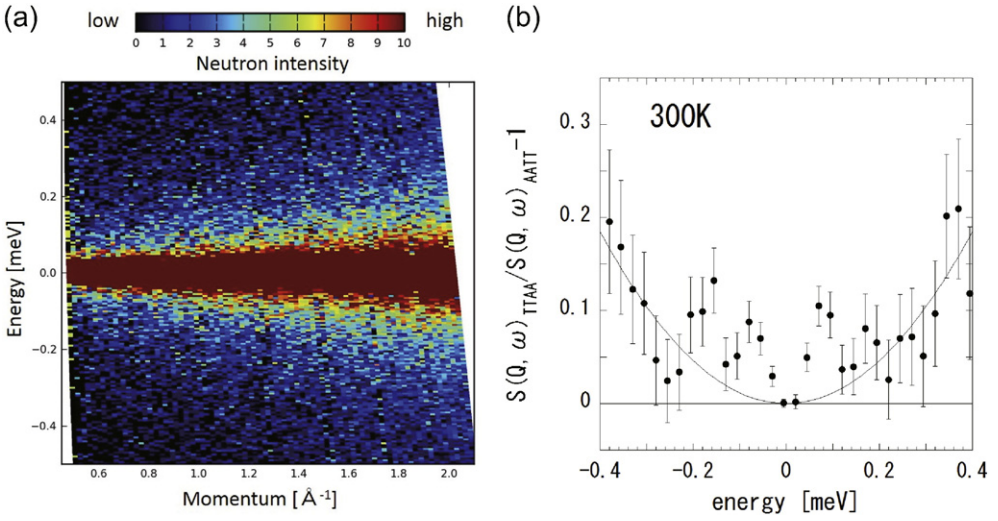

Fig. 14. (a) QENS spectra of a dodecameric DNA sequence, 5'CGCGAATTCGCG3' (b) Comparison of the ratio of quasi-elastic scattering intensity for TTAA to AATT at 300 K. The $S(Q,\omega)$ for AATT and TTAA are scaled by the intensity at the elastic position before the calculation of the ratio. The curve is a guide for eye.

6.2. Water molecules confined in lipid membranes

Dynamical properties of hydration water have attracted considerable interest from the viewpoint of biology, because these molecules play an important role in biological functions. For example, protein dynamics and folding are known to strongly depend on the dynamical behavior of hydration water [52,53,54].

Phospholipids, consisting of hydrophobic alkyl chains and hydrophilic head groups, are major components in biological membranes and form bilayer structures. The phospholipid membranes and their hydrated water have been studied intensively as model biomembranes. Hishida and Tanaka investigated the dynamical behavior of water in an aqueous solution of phospholipid 1,2-dimyristoyl-sn-glycero-3-phosphocholine (DMPC) by THz spectroscopy and showed that 28 water molecules were hydrated per one DMPC molecule corresponding to the hydrated layer of four or five, which is larger than expected [59]. From computer simulations of lipid bilayers, sub-diffusive and ballistic regimes of hydration water motions have been predicted [60,61]. NMR imaging showed that water molecules move anisotropically when diffusing parallel or perpendicular to the membranes [62]. From time-resolved vibrational spectroscopy, it was shown that water molecules in DOPC membranes is distributed anisotropically and forms nano-clusters [63].

QENS is a suitable tool to investigate water dynamics because it covers time scale from pico to nano second and has atomic scale resolution [55,56,57,58]. So far, QENS has been utilized to observe the dynamical behavior of lipid molecules in the DMPC/water mixture [64,65,66]. The water dynamics in this mixture is also investigated by QENS [67,68,69,70]. In these experiments, the contribution to QENS spectra from the methyl groups in the head group can not be neglected because the chain-deuterated DMPC (d_{54}DMPC) was used. Swenson et.al. tried to estimate the contribution from the head group by subtraction between the QENS data of d_{54}DMPC/H_2O and those of d_{54}DMPC/D_2O [67], however, it should be noted that the measured energy range was not suitable. Considering these situations, we used the fully deuterated DMPC (d_{67}DMPC) in order to investigate full dynamics of water molecules confined between lipid membranes at broader energy range with high energy resolution near-backscattering spectrometer DNA [35].

The sample was the mixture of d_{67}DMPC and H_2O in order to include 37 water molecules per DMPC molecule. For this sample, the incoherent scattering cross sections of the water and the DMPC are 80% and 7% of the total scattering, respectively. Therefore the neutron scattering intensity mainly reflects the dynamics of the water molecule. This amount of water corresponds to the full hydration between lipid bilayers [59]. The sample was prepared by mixing d_{67}DMPC powder with appropriate amount of water to form multi lamellar vesicles. The 105 mg sample wrapped with an aluminum foil, 30 mm height and 90 mm width, was put in the cylindrical aluminum can whose inner and outer diameters are 14 and 14.5 mm, respectively. The can was sealed with a metal O ring. The temperature was controlled within an accuracy of ± 0.1 K with standard sample environment of DNA spectrometer between 270 and 320 K. Three different fast chopper settings were used at each temperature in order to cover broad energy transfer between -0.4 and 0.6 meV. The energy resolution was set at 3.6 μeV. The counting time was ca 11.5 h at each temperature with three different chopper conditions.

Fig. 16(a) shows the QENS profile of the d_{67}DMPC-37H_2O at 0.63 $Å^{-1}$ and 317 K. The profile was well fitted by the following equation.

$$S(Q,E) = \{A_{Delta}\delta(E) + A_{Slow}L(\Gamma_{Slow},E)A_{Fast}L(\Gamma_{Fast},E)\}\otimes R(Q,E) + BG \quad (2)$$

A, δ, L, Γ, R and BG are constant, delta function, Lorentzian function, half width at half maximum (HWHM) of the Lorentzian function, resolution function and constant background, respectively. The obtained HWHMs shown in Fig. 16(b) follow random jump diffusion model, Eq. (1) [50].

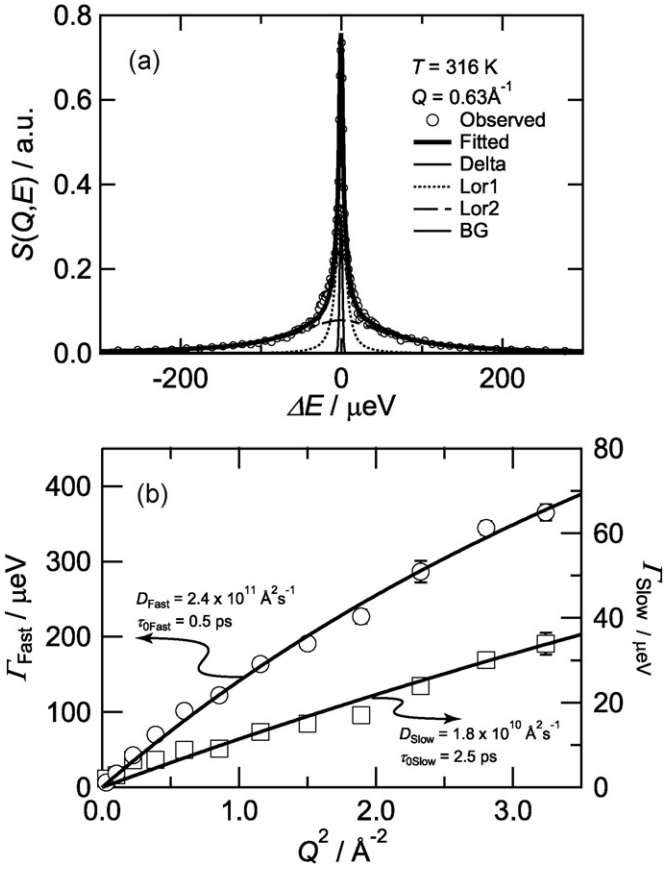

Fig. 16. (a) QENS profile of d_{67}DMPC-37H_2O at 0.63 $Å^{-1}$ and 317 K. The bold solid line is the result of fitting to Eq. (2). (b) The HWHM of the fast (circle) and slow (square) modes obtained by the profile fitting as a function of Q^2. The solid lines are the results of the fitting to Eq. (1).

The obtained diffusion coefficients and mean residence times are written in the figure. The water molecules confined between the lipid bilayer could be categorized into three types; free water having similar diffusion coefficients to that of bulk water ($D = 3.2 \times 10^{11}$ $Å^2s^{-1}$, $\tau_0 = 0.55$ ps at 313 K [58])(fast), loosely hydrated water having ca. one order of magnitude slower diffusion coefficients than that of the fast mode (slow) and strongly hydrated water to the DMPC head group (delta). Because the strongly hydrated water should move cooperatively with DMPC molecules, the delta component also includes the incoherent scattering from the DMPC although the contribution could be minor (7% of total scattering) [71]. The DNA spectrometer demonstrates the capability to observe broad range dynamics simultaneously such as, from the hydration water to the bulk water, in this experiment.

7. Conclusion

Since the start of the user program in 2008, J-PARC has gradually increased the proton beam power up to 500 kW and developed various kinds of instruments even though we had several long and short shutdown periods due to problems such as the great earthquake, the radio-active material leakage incident at Hadron Experimental Facility, the cooling water leakage at the neutron target, etc. The set of INS and QENS instruments in MLF has already become one of the top-class instrumental suites to investigate hierarchical dynamics including bio-related materials. Further developments of the facility and the instruments will give opportunities to push out the frontier of neutron science.

Transparency document

The Transparency document associated with this article can be found, in online version.

Acknowledgments

We are indebted to M. Arai at European Spallation Source for his leadership in the construction of MLF and the neutron instruments. We also thank T. Masuda and H. Yoshizawa at The University of Tokyo, K. Ohoyama at Ibaraki University, M. Hino, T. Oda and N. Takahashi at Kyoto University, M. Fujita at Tohoku University, Y. Yonetani and H. Kono at National Institutes for Quantum and Radiological Science and Technology, M. Kataoka at Nara Institute of Science and Technology and all the staffs of MLF for their contributions and collaborations to develop and improve these spectrometers. Neutron scattering experiments were performed under the MLF user program (Proposal No. 2012P0402, 2012I0002, 2013P0402, 2013I0002, 2014P0402, 2014A0108, 2014B0338, 2014I0001, 2014I0002, 2014I0014, 2009S01, 2009S07, 2009S09, 2010S01, 2011S01, 2012S01, 2013S01, 2014S01, 2014S07, 2014S09). The authors (K. Nakajima, T. Yamada and H. Nakagawa) were supported by JSPS KAKENHI Grant Numbers 24510133, 25790005, 22113521, 23650469.

References

[1] M. Arai, et al., Proc. 16th Meet. Int. Collaboration on Advanced Neutron Sources (ICANS-XVI), 2003 157.
[2] F. Tamura, M. Yoshii, A. Schnase, C. Ohmori, M. Yamamoto, M. Nomura, M. Toda, T. Shimada, K. Hara, K. Hasegawa, Nucl. Instrum. Methods Phys. Res., Sect. A 647 (2011) 25.
[3] T. Imae, T. Kanaya, M. Furusaka, N. Torikai (Eds.), Neutrons in Soft Matter, John Wiley & Sons 2011, p. 601.
[4] M. Harada, N. Watanabe, M. Teshigawara, T. Kai, F. Maekawa, T. Kato, Y. Ikeda, Proc. 17th Meet. Int. Collab. Adv. Neutron Sources (ICANS-XVII) 700, 2005.
[5] S. Ikeda, J.M. Carpenter, Nucl. Instrum. Methods Phys. Res., Sect. A 239 (1985) 536.
[6] R. Kajimoto, M. Nakamura, Y. Inamura, F. Mizuno, K. Nakajima, S. Ohira-Kawamura, T. Yokoo, T. Nakatani, R. Maruyama, K. Soyama, K. Shibata, K. Suzuya, S. Sato, K. Aizawa, M. Arai, S. Wakimoto, M. Ishikado, S. Shamoto, M. Fujita, H. Hiraka, K. Ohoyama, K. Yamada, C.H. Lee, J. Phys. Soc. Jpn. 80 (2011) SB025.
[7] Y. Inamura, T. Nakatani, J. Suzuki, T. Otomo, J. Phys. Soc. Jpn. 82 (2013) SA031.
[8] K. Iida, K. Ikeuchi, M. Ishikado, J. Suzuki, R. Kajimoto, M. Nakamura, Y. Inamura, M. Arai, JPS Conf. Proc. 1 (2014) 014016.
[9] M. Nakamura, R. Kajimoto, Y. Inamura, F. Mizuno, M. Fujita, T. Yokoo, M. Arai, J. Phys. Soc. Jpn. 78 (2009) 093002.
[10] F. Mezei, J. Neutron Res. 6 (1997) 3.
[11] F. Mezei, M. Russina, S. Schorr, Physica B 276–278 (2000) 128.
[12] K. Iida, M. Kofu, N. Katayama, J. Lee, R. Kajimoto, Y. Inamura, M. Nakamura, M. Arai, Y. Yoshida, M. Fujita, K. Yamada, S.-H. Lee, Phys. Rev. B 84 (2011) 060402(R).
[13] K. Nakajima, R. Kajimoto, Hamon 25 (2015) 39 (in Japanese).
[14] K. Nakajima, et al., J. Neutron Res. 15 (2009) 13.
[15] K. Nakajima, et al., J. Phys. Soc. Jpn. 80 (2011) SB028.
[16] K. Nakajima, et al., Proc. ICANS-XXI, JAEA-Conf **2015–002**, 2015 306.
[17] R.I. Bewley, et al., Nucl. Instrum. Methods 637 (2011) 128.
[18] G. Ehlers, et al., Rev. Sci. Instrum. 82 (2011) 085108.
[19] T. Kikuchi, et al., Phys. Rev. E 87 (2013) 062314.
[20] S. Itoh, T. Yokoo, S. Satoh, S. Yano, D. Kawana, J. Suzuki, T.J. Sato, Nucl. Inst. Methods Phys. Res. A 631 (2011) 90.
[21] S. Itoh, Y. Endoh, T. Yokoo, D. Kawana, Y. Kaneko, Y. Tokura, M. Fujita, J. Phys. Soc. Jpn. 82 (2013) 043001.
[22] S. Itoh, T. Yokoo, D. Kawana, Y. Kaneko, Y. Tokura, M. Fujita, K. Yoshida, K. Saito, N. Inami, Y. Takeichi, K. Ono, Y. Endoh, J. Phys. Conf. Series 502 (2014) 012043.
[23] L. Passell, O.W. Dietrich, J. Als-Nielsen, Phys. Rev. B 14 (1976) 4897.
[24] Y. Ishikawa, K. Yamada, K. Taijma, K. Fukamachi, J. Phys. Soc. Jpn. 50 (1981) 1958.
[25] R.A. Robinson, Physica B 156 & 157 (1989) 557.
[26] D. Aisa, S. Aisa, E. Babucci, F. Barocchi, A. Cunsolo, A. De Francesco, F. Formisano, T. Gahl, E. Guarini, A. Laloni, H. Mutka, A. Orecchini, C. Petrillo, W.-C. Pilgrim, A. Piluso, F. Sacchetti, J.-B. Suck, G. Venturi, J. Non-Cryst. Solids 352 (2006) 5130.
[27] Y. Endoh, K. Hirota, J. Phys. Soc. Jpn. 66 (1997) 2264.
[28] Z. Fang, N. Nagaosa, K.S. Takahashi, A. Asamitsu, R. Mathieu, T. Ogasawara, H. Yamada, M. Kawasaki, Y. Tokura, K. Terakura, Science 302 (2003) 92.
[29] K. Yoshida, T. Yamaguchi, D. Kawana, T. Yokoo, S. Itoh, MLF Annual Report 2013 (J-PARC 14–03, KEK Progress Report 2014-4), 2014 33.
[30] T. Yokoo, et al., J. Phys. Soc. Jpn. 82 (2013) SA035.
[31] T. Yokoo, et al., J. Phys. Conf. Ser. 502 (2014) 012046.
[32] T. Yokoo, K. Ohoyama, S. Itoh, K. Iwasa, N. Kaneko, J. Suzuki, M. Ohkawara, K. Aizawa, S. Tasaki, T. Ino, K. Taketani, S. Ishimoto, M. Takeda, T. Oku, H. Kira, K. Hayashi, H. Kimura, T.J. Sato, EPJ Web Conf. 83 (2015) 03018 (1–5).
[33] H.B. Stuhrmann, K.H. Nierhaus, Basic Life Sci. 64 (1996) 391.
[34] Y. Noda, et al., Phys. Procedia 42 (2013) 52.
[35] K. Shibata, N. Takahashi, Y. Kawakita, M. Matsuura, T. Yamada, T. Tominaga, W. Kambara, M. Kobayashi, Y. Inamura, T. Nakatani, K. Nakajima, M. Arai, JPS Conf. Proc. 8 (2015) 036022.
[36] S. Fujiwara, T. Yamada, T. Matsuo, N. Takahashi, K. Kamazawa, Y. Kawakita, K. Shibata, J. Phys. Soc. Jpn. 82 (2013) SA019.
[37] S. Fujiwara, K. Araki, T. Matsuo, H. Yagi, T. Yamada, K. Shibata, H. Mochizuki, PLoS One 11 (4) (2016) e0151447.
[38] F. Mezei (Ed.), Neutron Spin Echo, Lecture Notes in Physics, Vol. 128, Springer-Verlag, 1980.
[39] M. Hino, T. Oda, M. Kitaguch, N.L. Yamada, H. Sagehashi, Y. Kawabata, H. Seto, Phys. Procedia 42 (2013) 136.
[40] D. Richter, M. Monkenbusch, A. Arbe, J. Colmenero, Adv. Polym. Sci. 174 (2005) 1.
[41] Y. Nambu, J.S. Gardner, D.E. MacLaughlin, C. Stock, H. Endo, S. Jonas, T.J. Sato, S. Nakatsuji, C. Broholm, Phys. Rev. Lett. 115 (2015) 127202.
[42] C. Pappas, E. Lelievre-Berna, P. Falus, P.M. Bentley, E. Moskvin, S. Grigoriev, P. Fouquet, B. Farago, Phys. Rev. Lett. 102 (2009) 197202.
[43] J. Kindervater, N. Martin, W. Haeussler, M. Krautloher, C. Fuchs, S. Muehlbauer, J.A. Lim, E. Blackburn, P. Boeni, C. Pfleiderer, EPJ Web Conf. 83 (2015) 03008.
[44] M. Hino, H. Sunohara, Y. Yoshimura, R. Maruyama, S. Tasaki, H. Yoshino, Y. Kawabata, Nucl. Inst. Meth. A 529 (2004) 54.
[45] T. Oda, Doctoral Thesis, Kyoto University, Japan, 2016.
[46] M. Bleuel, M. Bröll, E. Lang, K. Littrell, R. Gähler, J. Lal, Physica B 371 (2006) 297.
[47] G. Brandl, J. Lal, J. Carpenter, L. Crow, L. Robertson, R. Georgii, P. Böni, M. Bleuel, Nucl. Inst. Meth. A 667 (2012) 1.
[48] Y. Yonetani, et al., Biophys. Chem. 160 (2012) 54.
[49] H. Nakagawa, et al., Phys. Rev. E 90 (2014) 022723.
[50] M. Bee, Quasielastic Neutron Scattering: Principles and Applications in Solids State Chemistry, Biology and Materials Science, Adam Hilger, Bristol, UK, 1988.
[51] W.K. Olson, et al., Proc. Natl. Acad. Sci. U. S. A. 95 (1998) 11163.
[52] P.W. Fenimore, et al., Proc. Natl. Acad. Sci. U. S. A. 101 (2004) 14408.
[53] H. Frauenfelder, et al., Proc. Natl. Acad. Sci. U. S. A. 103 (2006) 15469.
[54] G. Zaccai, Philos. Trans. R. Soc. London, Ser. B 359 (2004) 1269.
[55] L. Liu, S.-H. Chen, A. Faraone, C.-W. Yen, C.-Y. Mou, Phys. Rev. Lett. 95 (2005) 117803.
[56] K. Yoshida, et al., J. Chem. Phys. 129 (2008) 054702.
[57] N. Malikova, et al., J. Phys. Chem. C 111 (2008) 17603.
[58] T. Yamada, et al., J. Phys. Chem. B 115 (2011) 13563.
[59] M. Hishida, K. Tanaka, Phys. Rev. Lett. 106 (2011) 158102.
[60] Y. von Hansen, S. Gekle, R.R. Netz, Phys. Rev. Lett. 111 (2013) 118103.
[61] F.Y. Hansen, et al., J. Chem. Phys. 137 (2012) 204910.
[62] P. Waesterby, G. Oraedd, G. Londblom, J. Magn. Reson. 157 (2002) 156.
[63] L. Piatkowski, J. de Heij, H.J. Bakker, J. Phys. Chem. B 117 (2013) 1367.
[64] S. Busch, C. Smuda, L.C. Pardo, T. Unruh, J. Am. Chem. Soc. 132 (2010) 3232.
[65] M. Trapp, et al., J. Chem. Phys. 133 (2010) 164505.
[66] V.K. Sharma, et al., J. Phys. Chem. B 119 (2015) 4460.
[67] J. Swenson, et al., J. Chem. Phys. 129 (2008) 164505.
[68] M. Bai, et al., Europhys. Lett. 98 (2012) 48006.
[69] A. Miskowiec, et al., Europhys. Lett. 107 (2014) 28008.
[70] L. Toppozini, et al., Soft Matter 11 (2015) 8354.
[71] T. Yamada, N. Takahashi, T. Tominaga, S. Takata, H. Seto, (in preparation).